Revista EIA, ISSN 1794-1237 / Año XI / Volumen 11 / Edición especial N.1 / Mayo 2014 / pp. E47-E59
Publicación semestral de carácter técnico-científico / Escuela de Ingeniería de Antioquia —EIA—, Envigado (Colombia)

ONE STEP SYNTHESIS OF MAGNETIC PARTICLES COVERED WITH CASEIN SURFACTANT

Jeaneth Patricia Urquijo Morales[1]
Herley Casanova Yepes[2]
✉ Álvaro Luis Morales Aramburo[3]
Roberto Daniel Zysler[4]

ABSTRACT

The one-step coprecipitation method is used to obtain magnetic nanoparticles controlling the pH (10 and 12), and casein surfactant (CS) concentrations (1 % and 3 % (m/m)). CS has not been used so far for stabilizing magnetic iron oxide ferrofluids. The magnetic nanoparticles have a magnetite core with maghemite in surface, and a shell of polymer. The transmission electron images confirm the crystallinity, particle size distribution in the range of 5-10 nm, and the spinel structure of the nanoparticles. Mössbauer results at 80 K showed line shapes dominated by magnetic relaxation effects with sextets and combinations of sextets and doublets. The interactions of the surfactant with the nanoparticle surface are strong showing at least two surfactant layers. The magnetic behavior was evaluated by moment versus temperature and magnetic field measurements. The nanoparticles showed superparamagnetic behavior at room temperature and blocked (irreversible) behavior at 5 K. The saturation magnetization presented lower values than reported bulk systems due to the presence of a large layer of maghemite. The FC/ZFC magnetization vs. temperature curves confirmed the superparamagnetic nature of the iron oxide particles and the strong interactions for pH 12 samples and weak interactions for pH 10 samples. The particle growth was dominated by the surface properties of the nanoparticles.

KEYWORDS: Magnetic Nanoparticles; Sodium Caseinate; Magnetic Measurements; Mössbauer Spectroscopy; FTIR, TGA.

SÍNTESIS DE PARTÍCULAS MAGNÉTICAS CUBIERTAS CON CASEINATO DE SODIO

RESUMEN

Se usa el método de coprecipitación para obtener nanopartículas magnéticas controlando el pH (10 y 12) y la concentración del caseinato de sodio (CS) (1 % y 3 %(m/m)). CS no se ha utilizado hasta el momento para estabilizar ferrofluidos magnéticos. Las partículas muestran un núcleo de magnetita, una capa de maghemita sobre el mismo, y otra capa exterior de la proteína. La microscopía electrónica de transmisión muestra partículas cristalinas, una distribución de tamaños entre 5-10 nm, y la estructura de espinela. Los resultados Mössbauer a 80 K muestran formas de línea

[1] Química, Universidad de Antioquia; MSc. en Ciencias Químicas, Universidad de Antioquia UdeA, Medellín (Colombia).

[2] Químico Universidad de Antioquia; PhD. en Química, Universidad de Leeds (Inglaterra); docente, Universidad de Antioquia UdeA; Grupo Coloides, Instituto de Química, Facultad de Ciencias Exactas y Naturales, Universidad de Antioquia, Medellín (Colombia).

[3] Físico, Universidad de Antioquia; PhD. en Física, Universidad de Lund, Suecia; docente Universidad de Antioquia; Grupo de Estado Sólido, Instituto de Física, Facultad de Ciencias Exactas y Naturales, Universidad de Antioquia UdeA, Medellín (Colombia).

[4] Licenciado en Física, Instituto Balseiro - Universidad Nacional de Cuyo; PhD. en Física, Instituto Balseiro - Universidad Nacional de Cuyo; investigador Principal, Consejo Nacional de Investigaciones Científicas y Técnicas (CONICET), Argentina; Profesor Asociado, Instituto Balseiro-Universidad Nacional de Cuyo, Argentina.

✉ *Autor de correspondencia:* Morales-Aramburo, A.L.: Universidad de Antioquia UdeA; Calle 70 N. 52-21, Medellín (Colombia). Teléfono: (574) 2195630.
Correo electrónico: amoral@fisica.udea.edu.co

Historia del artículo:
Artículo recibido: 26-XI-2012 / Aprobado: 11-VII-2013
Discusión abierta hasta diciembre de 2014

DOI: http:/dx.doi.org/10.14508/reia.2013.10.20.13-22

dominadas por efectos de relajación magnética. La interacción de la proteína con la superficie de las nanopartículas es fuerte y muestra varias capas de proteína. El comportamiento magnético se evaluó mediante medidas termomagnéticas y de momento versus campo magnético. Estas revelaron un sistema superparamagnético a 300 K y bloqueado a 5 K. La magnetización de saturación mostró valores menores que en el volumen posiblemete debido a la presencia de la maghemita. Las medidas termomagnéticas confirmaron el superparamagnetismo y mostraron que las muestras obtenidas a pH 12 presentan interacciones fuertes mientras que las de pH 10 muestran interacciones débiles. El crecimiento de las partículas fue dominado por las propiedades superficiales de las partículas.

PALABRAS CLAVES: nanopartículas magnéticas; caseinato de sodio; medidas magnéticas; espectroscopia Mössbauer; FTIR; TGA.

SÍNTESE EM UM PASSO DE PARTÍCULAS MAGNÉTICAS COBERTAS COM SURFACTANTE CASEINA

SUMÁRIO

O método de co-precipitação numa etapa utiliza-se para obter nano partículas magnéticas que controlam o pH (10 e 12), e a concentração do surfactante caseína (1 % and 3 %(m/m)). CS não foi usado para estabilizar os ferrofluidos óxidos magnéticos. As nanopartículas magnéticas tem um centro magnético com maghemite em superfície e uma casca de polímero. As imagens de transmissão de eléctron confirmam a cristalinidade, a distribuição das partículas dum tamanho de 5-10 nm, e a estrutura de espinela das nanopartículas. Os resultados de Mössbauer a 80 K mostraram formas de linhas dominadas por efeitos de relaxação magnéticas com sextetos e combinações de sextetos e duplicados. A interações do surfactante com a superfície da nanopartículas são fortes e mostram mínimo dois camadas de surfactante. O comportamento magnético foi avaliado em momentos versus temperatura e medidas de campo magnético. As nanopartículas mostraram comportamento superparamagnético com a temperatura de estudo e bloquearam (irreversível) a 5 K. A saturação da magnetização apresentou valores menores que os valores reportados nos sistema a granel devido à presença duma grande camada de maghemite. A magnetização FC/ZFC vs. Curvas de temperatura confirma o estado superparamagnético das partículas de óxidos de ferro e as fortes interações das amostras pH12 e as fracas interações das amostras pH 10. O crescimento das partículas foi dominado pelas propriedades das superfícies das partículas.

PALAVRAS-CHAVE: nanopartículas magnéticas; sodium caseinate; medidas magnéticas; spectroscopia Mössbauer; FTIR; TGA

INTRODUCTION

Iron oxide magnetic nanoparticles, particularly mixtures of magnetite and maghemite, have been synthesized by different routes for more than one decade (Gupta and Gupta, 2005; Roca, *et al*., 2009; Zhai, *et al*., 2009). The goal is to apply them in industry and biomedicine (Herzera, *et al*., 2005). The colloidal stability is of primary importance to ensure the proper performance of the ferrofluids and also to further functionalization of the physical-chemical system. Issues about biocompatibility and biodegradability have been also addressed. Prozorov, *et al*. (2007) have used various proteins to synthetize magnetite, one is related to the biomineralization of bacterial magnetite magnetosomes (BBMM), and others are the mammalian iron-storage protein, ferritin, lipocalin and bovine serum albumin. They used the coprecipitation method with the presence of the protein and introduced a polymeric gel to slow down the reaction. With the BBMM, they obtained uniform magnetite crystals of around 30 nm diameter with good magnetic properties, the other proteins produced non-uniform nanoparticles. Amemiya, *et al*. (2007) also used BBMM but a different synthesis route obtaining uniform magnetite nanoparticles with cubo-octahedral morphology.

Sugiarto and Singh (2009) had studied the binding of iron, from ferrous sulfate, to sodium caseinate (CS) and whey protein as a function of pH in the range 5.5-7, if the pH is decreased the iron binding decreases. They found that CS has more sites to bind iron than whey protein, which is important to the fortification of dairy products with iron and also shows the potential use of casein as a stabilizer of iron oxide nanoparticles.

Zhai, *et al*. (2009) have synthetized magnetite in acrylic acid anion at concentrations smaller than 0.5 % (m/m), obtaining sizes between 12-20 nm and confirming by FTIR and TGA that the anion has been attached to the surface in a chelating bidentate configuration. Barbeta, *et al*. (2010) obtained almost spherical 5.5 nm diameter magnetite particles from a so-gel method. The nanoparticles were covered with two substances, oleic and dodecanoic acids, with a concentration of magnetite in the range 63-78 % and saturation magnetization ranging from 83.2-96.0 emu/g, these high values are explained as an effect of the acids preventing surface spin disorder. Also, they found that interparticle dipolar interactions were important due to their high magnetite concentration. Dallas, *et al*. (2006) obtained poly(methyl methacrylate) or polystyrene/magnetite nanocomposites, the polymers were added after the magnetic particles were formed. For the 32 % wt and 6 % wt iron oxide samples the saturation magnetization was 13 and 3 emu/g and coercitivity 240 and 220 Oe respectively. The particles showed a cubic morphology with 20 nm average size.

Nadeem, *et al*. (2011) have simulated theoretically the interparticle interactions in field cooling (FC) measurements and they found a flattening of the FC curve at low temperatures as a signal of such interactions; for monodisperse particles the FC curve increases monotonically as the temperature decreases. They also produced 4 nm average maghemite nanoparticles by microwave plasma method from which they obtained monodisperse and compacted samples. The FC experimental curves were in agreement with the computer simulations. Tetramethyl ammonium hydroxide (TMAOH)-functionalized 8 nm nanoparticles were obtained by Rebodos and Vikesland (2010) using the one-step coprecipitation method. They found, by oxidizing the nanoparticles to drive the transformation from magnetite to maghemite, a decrease in the saturation magnetization. This effect also helped to improve colloidal stability due to the decreased magnetic interaction between them.

In the present study the one-step coprecipitation method is used to obtain magnetic nanoparticles at controlled pH of 10 and 12, and sodium caseinate (CS) surfactant concentrations of 1 % and 3 % (m/m). CS is a mixture of water soluble lactic proteins and aminoacids which provide superficial charges distributed along the peptide chain. It is also biocompatible and biodegradable, necessary attributes for biological applications. CS has not been used so far; however, while this paper was written a reference by Huang, *et al*. (2013) appeared where they used a two-step method to cover the iron oxide nanoparticles with CS. Their emphasis was on the application as a magnetic resonance image contrast agent while the present study focuses on the characterization of the system and control of the synthesis. CS provides the required electrosteric properties to stabilize the nanoparticle fluid, and at the same

time, the surfactant adheres to the nanoparticle surface providing a way to further functionalize the system. Furthermore, CS is intended as a means of controlling the nanoparticle growth.

EXPERIMENTAL

The magnetic nanoparticles were obtained by the coprecipitation method (Lin, *et al*. 2005), starting with precursors $FeCl_3.6H_2O$ (≥99 %), $FeCl_2.4H_2O$ (≥99 %) y NaOH (≥99 %) obtained from Merck®, and food grade CS. All solutions were prepared and the synthesis ran under nitrogen flux in order to avoid oxidation. Also deionized water was used in the solution preparation. A 0.06 M solution of Fe^{2+}, a 0.12 M solution of Fe^{3+}, and a 2M solution of NaOH were poured into a solution of the surfactant with automatic pH control using a Metrohm 907. Magnetic stirring of the solution was kept at room temperature, 21-23 °C, during all the synthesis time. The black product was washed using a dialysis membrane until the conductivity of the water was the same as the conductivity of deionized water. The nanoparticles embedded in the protein were dried using mechanical vacuum. Part of the solutions were converted to gel by adding 0.2 g/ml agar, to preserve the particle distribution in the fluid. The same synthesis was repeated without the surfactant to obtain a set of nanoparticles as a reference. The synthesis was carried out for pH of 10 and 12 and surfactant concentrations of 1 % and 3 % (m/m), the samples were named as concentration-surfactant-pH, e.g. 3-CS-10 (3CS10), etc. The synthesis solution became very viscous, due to the high surfactant concentration which brought some problems with the magnetic stirring.

In order to assess the amount of iron in the samples, i.e. the amount of magnetite/maghemite, Atomic Absorption Spectroscopy (AAS) was used. To corroborate the phase composition of the obtained product, magnetite and maghemite, Micro-Raman (MR) measurements were taken in a Horiba Jobin Yvon, model Labram HR with CCD detector with resolution of 1024x256 pixels, spectral range of 100-500 cm^{-1} and a 633 nm He/Ne laser. The crystalline structure of the spinel phases was probed by X-ray diffractograms taken with CuKα radiation in the range 10-80 2θ, step 0,02 2θ, 3 seconds per step. The XRD analysis was performed with the Powderx program by Dong (2000) and observed peaks were assigned according to the JCPDS cards (2001). The morphology and particle size distribution were examined by Transmission Electron Microscopy (TEM) with a Philips CM200 UT microscope, operating at 200 kV. Magnetic information on the samples was obtained by means of the Mössbauer technique in a Wissel spectrometer with MR-260 transducer, ^{57}Co (Rh) source, and a closed-cycle cryostat, the hyperfine parameters were extracted by the DISTRI program (Vandenberghe, *et al*.,1994).

All spectra were fitted with hyperfine field and quadrupole splitting distributions due to the asymmetric line shape found. The sextet spectra for the pH 12 samples were fitted using a modification of the model by Berry *et al*. cited in Doriguetto *et al*. (2003) which consists of five iron sites: Fe^{3+} (F3T) from tetrahedral sites, Fe^{3+} (F3O) from octahedral sites, a mixed-valence $Fe^{2.75+}$ (F32O) from octahedral sites, Fe^{2+} (F2O) from octahedral sites, and a Fe^{3+} (F3S) sextet coming from the surface of the particles. This site was included because the spectra showed a feature different from the spectra reported in the previous reference. The interaction of the surfactant with the surface of the nanoparticles was sensed by both Fourier Transform Infrared Spectroscopy, in a Perkin Elmer equipment, and thermogravimetric analysis, in a T.A Instruments Q100 v. 9.9. Further, magnetic characteristics of the samples were analyzed by magnetic field versus magnetic moment and thermomagnetic measurements in a Quantum Design PPMS, Vibrating Sample Magnetometer, in the temperature range 5-300 K.

RESULTS AND DISCUSSIONS

Table 1 shows the results for the dried samples studied from atomic absorption spectroscopy; the

Table 1. Atomic absorption for all samples

Casein	% magnetite ±0.1
1 CS12	93.5
1 CS10	38.3
3 CS12	67.0
3 CS10	28.7

Table 2. Comparison of observed Raman modes (cm^{-1}.) for the nanoparticles

Fe_3O_4	PpH12	1CS12	1CS10	3CS12	3CS10	Assignment
315	329	323			317	Eg
374		381		381	369	g-Fe2O3
445	420	430	429	460	438	T2g
530	522		545		546	T2g
627	627	627	627	627	627	g-Fe2O3
664	665	670	672	674	672	A1g
712	709	716	707	707	705	Fe(III)b
	687	680				Interface

percentage is calculated assuming that all iron is present in the magnetite phase, although there is an unknown layer of maghemite.

After drying the system it resembles a plastic with the nanoparticles embedded in it. It is seen that the magnetite percentage (mass to mass) is the largest for 1CS12 and decreases in the order 3CS12, 1CS10, and 3CS10. As a general trend, it can be said that the iron oxide content is larger for pH 12 samples. Of course, there is a layer of the protein covering the samples. The amount of surfactant deposited on the particle surface can be understood considering the negative charge increase on the particles and on the protein surface as the pH increases leading to a larger electrostatic repulsion for pH 12, since magnetite and casein are well above the point of zero charge (PZC). Furthermore, additional binding mechanisms are acting in those systems like steric repulsion, Van der Waals forces, surface complexing and formation of hydrogen bridges. The layers over the nanoparticles will play an important role for applications since functionalizing substances can be added on them.

The nanoparticles grew as a mixture of magnetite and maghemite, i.e. there was an oxidation process during the synthesis, and they underwent further oxidation due to the drying process. Micro Raman Spectroscopy was used to obtain information about this mixture. **Table 2** shows the strongest peak positions for all samples according to the literature (Soler and Qu, 2012).

The uncovered sample PpH12 shows a similar spectrum with peaks corresponding to magnetite and maghemite. The main structure around 600-800 cm^{-1} is broad due to particle size distribution in the samples and to overlapping phases. Also, this structure is composed of three peaks at around 665 cm^{-1}, 680 cm^{-1} and 709 cm-1. The first peak corresponds to magnetite; the third peak has been assigned to iron oxidation (Soler and Qu, 2012) at the magnetite B-sites, i.e. non-stoichiometric magnetite, but other authors assigned it to maghemite (Slavov, *et al.*, 2010). The peak at 680 cm^{-1} has not been reported in the literature as a peak belonging to magnetite or maghemite but it may come from the interface magnetite-maghemite.

The Raman spectra of covered samples show essentially the same features as the plain sample, i.e. the presence of the two phases, magnetite and maghemite, and broad peaks indicating the presence of particle size distributions. There is a noticeable trend for the amount of the maghemite phase to be smaller for pH 10; in this way the surfactant was protecting the nanoparticles from further oxidation.

X-ray diffraction is shown in **Figure 1** for selected samples. It shows only spinel peaks belonging to both magnetite and maghemite not separable by this technique, confirming the Raman results. Main peaks are found at 30.16, 35.52, 43.17, 53.56, 57.10, 62.70 2Θ (from JCPDS card 88-0315). The peaks are broad due to the small particle size of the samples, this broadening leads to crystallite sizes, by using the Scherrer's formula with an error of 10 %, of 13 nm and 11 nm for 1CS12 y

Figure 1. X-ray diffraction spectra for pH 12 samples and reference PpH12

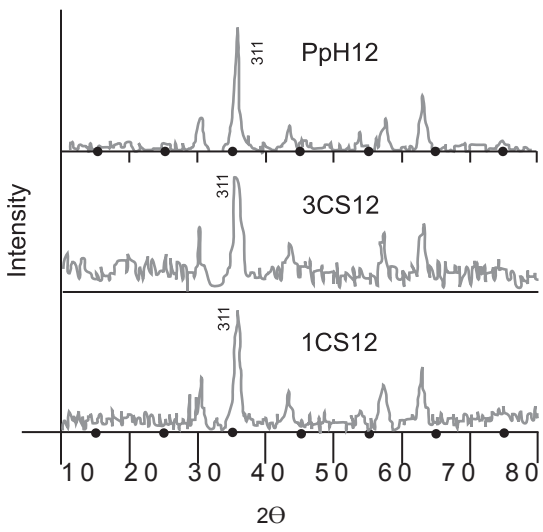

3CS12 samples respectively. For this kind of superparamagnetic particles the sizes given by XRD, TEM, and magnetic measurements are very close (Goya, 2004).

TEM spectra were recorded in order to confirm the particle morphology, for the selected sample 3CS12, the results are shown in **Figures 2-4. Figure 2** (upper) depicts the crystal planes of the particles indicating well crystallized particles; close to the borders the particle image looks blurred due to the protein surrounding the particles. **Figure 2** (lower), taken at a larger scale, shows the broad particle size distribution. This is in agreement with the discussion given above for the Raman results. In **Figure 3** a picture is shown at an intermediate TEM scale and a plot of the particle size distribution was obtained. The solid line is a fit to a log-normal distribution and with a mean of 7 nm diameter and a standard deviation of 2 nm. **Figure 4** shows a selected area electron diffraction spectrum (SAED), which displays a polycrystalline response and confirms the presence of nanoparticle aggregates in the samples. The ring radii of 0.290 nm, 0.246 nm, 0.204 nm, 0.159 nm, and 0.149 nm confirm the presence of magnetite/maghemite, in agreement with MR and XRD. The corresponding diffracting spinel planes correspond respectively to (2 0 0), (3 1 1), (4 0 0), (5 1 1), and (4 4 0). These results are in agreement with Alexandrescu, *et al.* (2008) and Zhang, *et al.* (2007).

The Mössbauer results, for dry samples, at 80 K are shown in **Figure 5** and hyperfine parameters are shown in **Table 3.**

The spectra are composed of sextets for pH 12 samples. The sextets show dominant components of Fe3+ and smaller components of mixed valence Fe2.75+ (IS=0.54 mm/s). At the lower pH of 10 a main superparamagnetic doublet and a magnetic component are present in the spectra; the sextets are dominated by Fe3+. It must be emphasized that the Mössbauer spectra line shape could be affected by interparticle interactions, due to the particle density in the polymer, as shown by AAS (**Table 1**), i.e. for the highest particle densities sextets are found and for the lower ones superparamagnetic doublets and small magnetic components are observed. These results mean that although the particles are small in size, or superparamagnetic, due to the high particle densities they interact by means of dipole-dipole interactions and produce a magnetic signal, recall the Scherrer crystallite size and TEM results mentioned

Figure 2. TEM results for sample 3CS12 showing crystalline particles and its size distribution

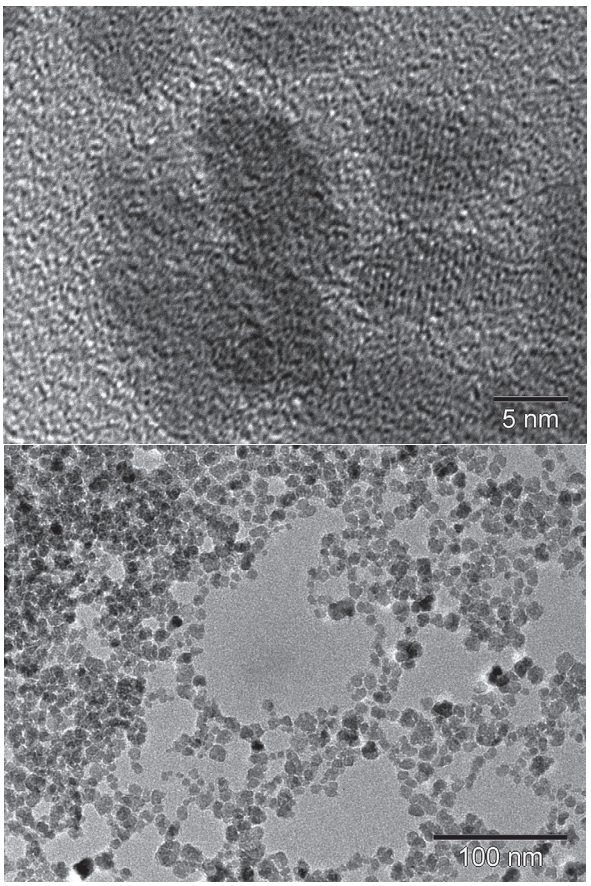

Figure 3. TEM for 3CS12 and the corresponding particle size distribution

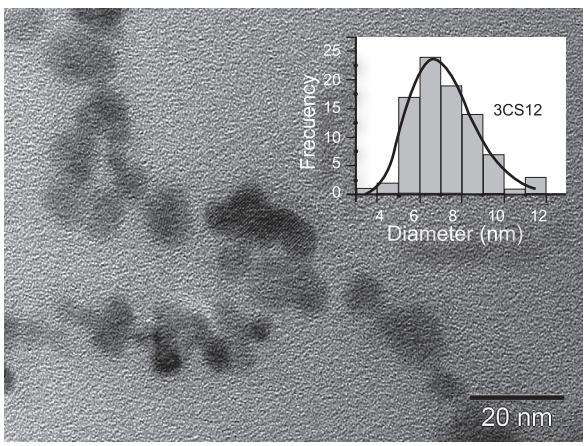

Figure 4. SAED diffraction pattern for sample 3CS12

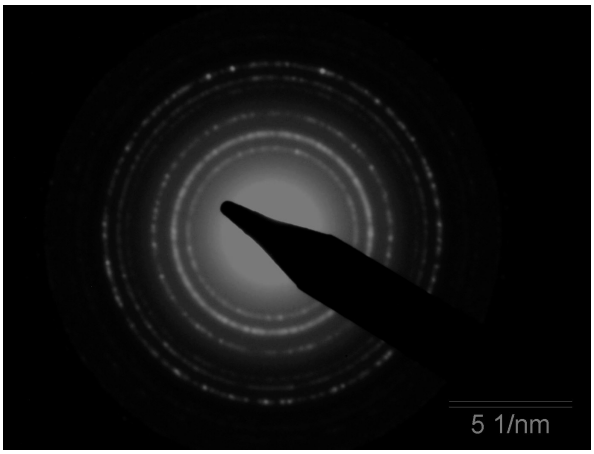

above. As a consequence, the Mössbauer line shape is attributed mainly to the presence of interparticle interactions and not to large magnetic particles (Novakova, *et al.*, 2006). In general, for large iron oxide particles, the crystallite size derived from XRD is smaller than the size given by TEM so the particles are polycrystalline (Morales, *et al.*, 2011).

The interaction of the magnetic particles with the protein was studied using FTIR. The results for the plain particles and the surfactant are shown in

Figure 5. Mossbauer spectra of selected samples

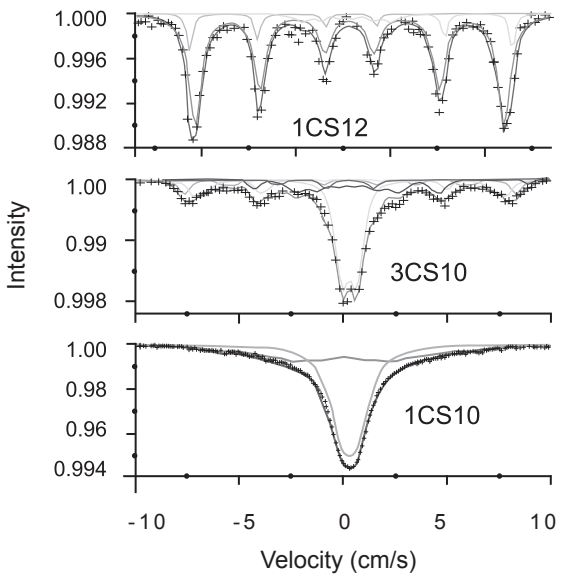

Figure 6. Table 4 summarizes the FTIR results for the four covered samples.

For the CS samples FTIR shows broadening, frequency shifts and intensity changes of the absorption bands. The amide bands I, II, and III are the most characteristic of this system. They are related respectively to the carbonyl group C=O stretching mode at 1640 cm^{-1},

Table 3. Hyperfine parameters for selected samples

Sample	Site	IS (mm/s) ±0.02	ΔQ (mm/s) ±0.02	B average (T) ±0.01	B Maximun (T) ±0.01	Area % ±4
1CS12	F3T	0.46	0.01	50.70	50.70	78
	F3O	0.31	0.00	15.19	14.17	6
	F32O	0.54	0.00	52.92	52.85	12
	F3S	0.44	-0.01	45.96	47.12	4
1CS10	Sextet	0.11	0.01	24.02	12.88	36
	Doublet	0.41	0.67			64
3CS10	F3T	0.46	0.01	49.49	49.47	12
	F3O	0.31	0.00	15.24	15.24	19
	F2O	0.31	0.01	35.70	33.20	7
	F3S	0.44	0.01	45.08	46.96	22
	Doublet	0.41	0.31			40

Table 4. FTIR bands(cm $^{-1}$) for casein covered samples

SAMPLE	Magnetite		Maghemite	PEPTIDIC BOND		
	ν(Fe-0)	δ(Fe-0)	ν(Fe-0)	Amida I	Amida II	Amida III
Pure	580(A)	440(B)	630	1640	1533	1200-1400
1CS12	584	439	630	1639	1515	1384
3CS12	587	441	627	1639	1527	1235
1CS10	577-595	452		1627	1514	1398
3CS10	537	452		1648	1559	1393

Figure 6. FTIR for casein covered samples

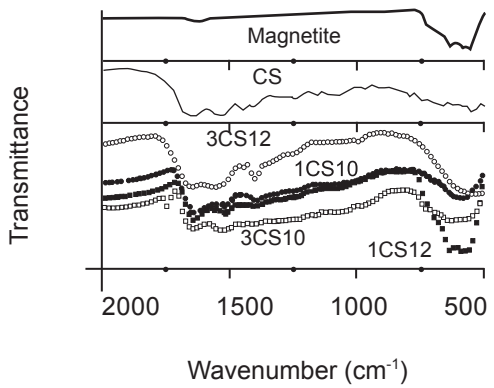

Figure 7. TGA for casein covered samples

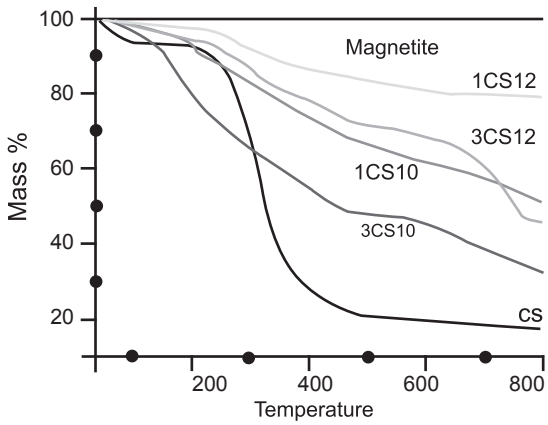

the combination of the flexion mode of N-H with the stretching mode of C-N at 1533 cm^{-1}, and the vibration of the C-N mode in the range 1200-1400 cm-1 (Barth, 2007; Koong and Yu, 2007; Barth and Zscherp, 2000). At the pH studied both the particles and casein have a negative surface; they are far beyond the PZC leading to a repulsive interaction between them. In this way, the binding of the casein to the particles proceeded mainly through the formation of chelates between phosphates groups and the Fe^{3+} at the surface of the particles. For the 3 % concentration samples, 3CS12 and 3CS10, there are frequency shifts for the amide II band, peak broadenings for amide I and II, and a relative intensity change, while for the 1 % concentration samples, 1CS10 and 1CS12, there are frequency shifts and intensity changes for amide I-II. For sample 1CS10 a sharpening of the amide bands is found but also some broadening which may mean the formation of a strong chelating binding to the particle surface. Also, the presence of the two phases, magnetite/maghemite (A and B are the spinel sites), is confirmed by the clearly seen peaks belonging to these phases, especially for pH 12 samples having the smaller amount of protein.

The thermogravimetric analysis allows the quantification of the adsorption of the protein to the magnetic nanoparticles. Figure 7 shows the TGA for pure magnetite and casein. Magnetite presents a small mass loss of 2.2 % due to physisorbed water, while casein presents two losses: one starting at room temperature until 150 °C due to water desorption, and a second one in the range 150-450 C, 71.8 %, due to the protein pyrolysis. The covered samples show an initial mass loss due to water desorption and a second process where

Table 5. magnetic parameters for the samples, PpH10 is a reference sample at pH 10

Sample	5K		300K		χi
	Ms (emu/g)	Hc(Oe) ±10***	Ms (emu/g)	Hc(Oe) ±10***	
Magnetite	96**		85-100*		
Maghemite	87**		74**		
PpH10	75.86	323	70.17	13	
1CS12	62.84	245	54,45	25	0.1062
1CS10	40.50	253	28.96	24	0.0358
3CS12	49.88	266	42.35	25	0.0904
3CS10	16.76	227	10.59	16	0.0113

Bulk values are from, * Haiping *et al*., 2009, ** Goss (1988), *** are error bars from Quantum Design

Figure 8. Hysteresis loops for all samples taken at T = 5K and T = 300K

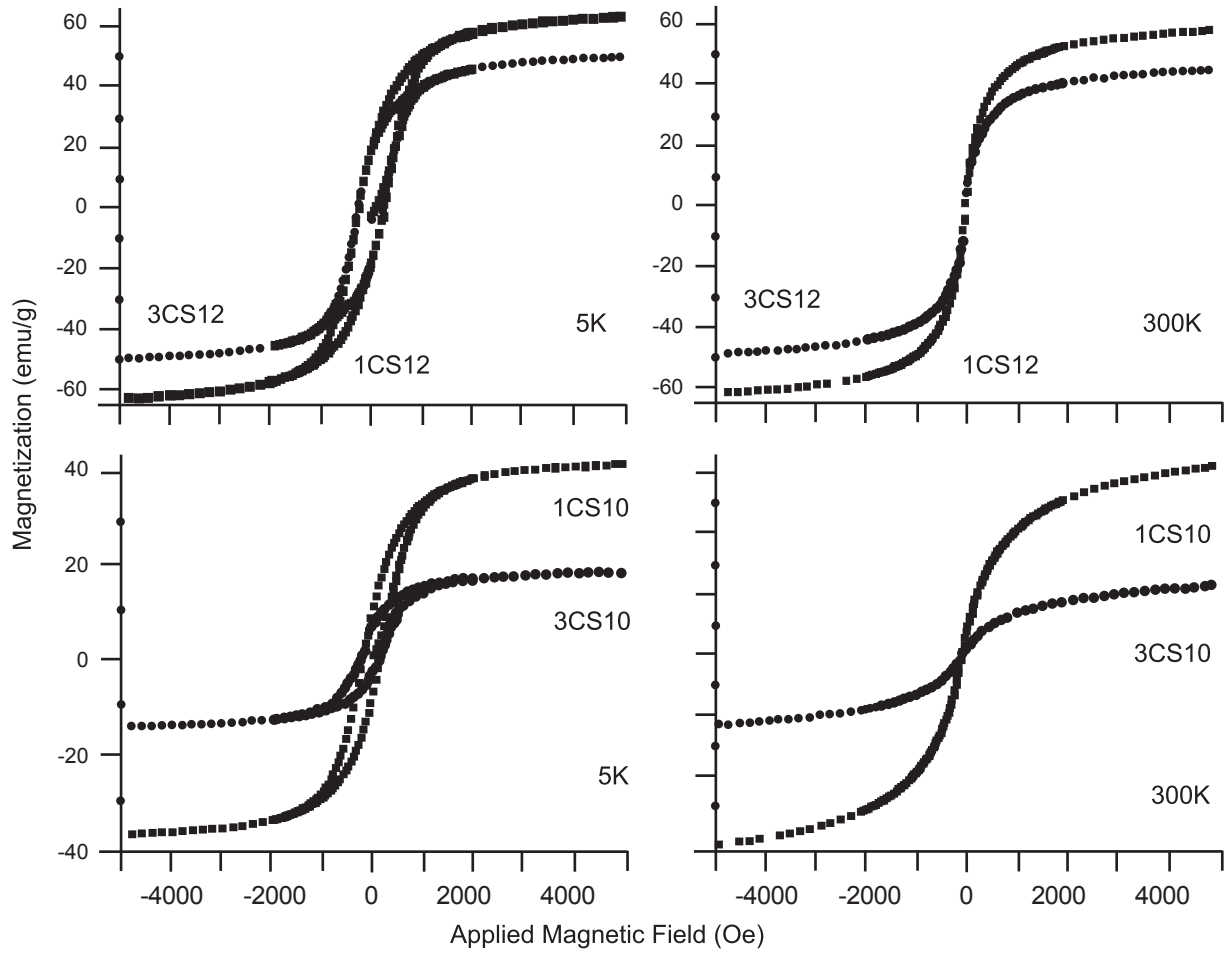

Table 6. Particle sizes by different techniques

sample	TEM(nm)	XRD (nm)	d_{mag}(nm)
3CS12	7	11	9
1CS12		13	9

Table 7. Blocking and irreversible temperatures from FC/ZFC

Sample	T_i	T_{max}	T_b	Mossbauer 80K(Table 4)
1CS12	190	168	52	sextet
1CS10	95	55	20	Doublet-small sextet (36 %)
3CS12	165	143	50	sextet
3CS10	64	40	17	Doublet-sextet (60 %)

Figure 9. FC (squares) and ZFC (solid dots) magnetization curves versus temperature for the samples

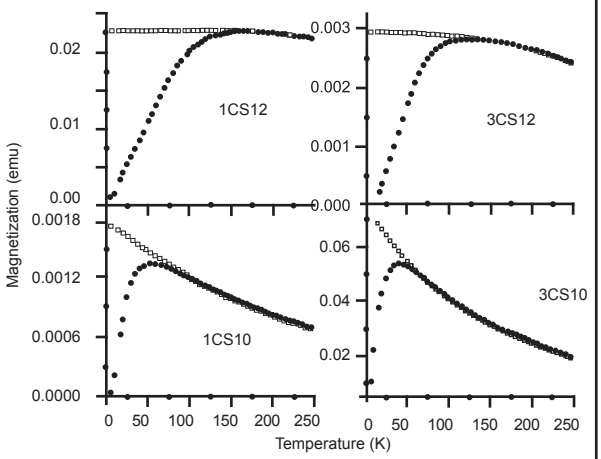

the protein pyrolysis extends to temperatures of 800 °C. This behavior is due to the different layers of the protein formed on the nanoparticles surface: the outermost layer decomposed first, the intermediate layer second, and the innermost layer is more difficult to decompose.

The magnetic behavior of the nanoparticles was analyzed by hysteresis and thermomagnetic measurements. It is important to remember that the samples were prepared as gels so as to freeze the particle distribution in the fluid. The gelification would influence the results making them different from some of the results shown above for powder dried samples, for which an extra oxidation took place. The results are shown in **Figure 8** and **Table 5** for moment versus field measurements.

The main characteristic at 300 K was the superparamagnetic behavior of the samples in contrast to 5 K where they behaved as ferrimagnetic. These small coercive field observed at room temperature is probably due to a tiny magnetic component coming from particle aggregation that occurred during the magnetic stirring of the highly viscous liquid and/or the presence of small amount of larger particles. The magnetic saturation is the largest for 1CS12 and decreases in the order: 3CS12, 1CS10, 3CS10, the same order as the amount of iron oxide given in **Table 1**. A similar magnitude order is found at 5 K. The magnetic saturation is considerably smaller than reported bulk values. These smaller magnetic saturations compared with reported values (Barbeta, *et al.*, 2010; Harris, *et al.*, 2003) are due to the maghemite layer surrounding the magnetite core in agreement with Rebodos and Vikesland (2010). From the measured initial susceptibility a rough estimation of the magnetic particle size, corresponding to the largest particles present in the distribution, can be made using the formula, where K_B , T, X_i , $\mu 0$, M_s, M_B , stand for the Boltzmann constant, temperature, initial susceptibility, vacuum permeability, saturation magnetization for nanoparticles, and saturation magnetization for bulk magnetite.

The magnetic particle size is presented in **Table 6** that shows how the particle size obtained from these samples is very similar in spite of the different synthesis conditions. This result indicates that the surface properties of the nanoparticles are the dominant factor by which the surfactant binds to it. Hence, the chelating mechanism by which the surfactants stick to the Fe^{3+} sites is confirmed.

The FC/ZFC magnetization measurements, **Figure 9,** give more detailed information on the particle size distribution and interparticle interactions. In these curves, the temperature of the maximum of the ZFC magnetization, T_{max}, related to the blocking temperature (~volume) distribution, and the irreversible temperature Ti where the FC curve starts to be above the ZFC curve, gives information about the distribution of magnetic energy barriers in the sample, **Table 7.**

A larger difference between T_{max} and T_i means a broader particle size distribution. The derivative gives the features of the magnetic energy barrier distribution highly correlated to the particle size distribution and also, the T_b value of the maximum of the barrier distribution (proportional to the volume distribution). **Table 7** shows large differences between T_{max} and T_i, with a corresponding wide derivative for the pH 12 samples and the opposite behavior for the pH 10 samples. With respect to interparticle interactions the pH 12 samples show strong forces and the pH 10 samples present very weak interactions. These interactions are also reflected in the increase of T_{max} for pH 12 samples. On the other hand, the flattening of the FC curve at low temperatures is indicating strong interactions between nanoparticle moments related to the large content of iron oxide (see **Table 1**). These results agree with Lima, *et al.* (2010) and Parker, *et al.* (2005).

It is worth noting that the 80 K Mössbauer spectra shown in **Figure 5** was composed of magnetic components in some cases and magnetic-superparamagnetic components for the other cases. A correlation can be drawn with the FC/ZFC magnetic measurement although the samples for the Mössbauer technique were in powder form while for magnetic measurements were gels. Sextets were obtained for the samples for which the 80 K temperature (T80) was below T_{max}, i.e. pH 12 samples. For 1CS10, T80 is in the middle of Tmax and Ti meaning that some moments are aligned and a magnetic component is expected. For 3CS10, T_{max} and T_i are well below T80 and a doublet should be expected, instead a sextet-doublet line shape appears pointing to the different sample preparation for which the powdering process allows the particle aggregation and further oxidation to maghemite.

CONCLUSIONS

TThe one step coprecipitacion, with the surfactant included, produced magnetic nanoparticles covered with significant amount of protein, especially for the pH 10 samples, as shown by absorption spectroscopy measurements. The magnetic nanoparticles have a magnetite core, and possibly a layer of non-stoichiometric magnetite, surrounded by a maghemite layer and a surfactant layer on top of that, as indicated by Raman, XRD, FTIR, TGA, and magnetic measurements. The maghemite layer is smaller for pH 10 samples. The TEM images confirm the crystallinity of the nanoparticles, their particle size distribution in the average range of 5-10 nm, and their spinel structure of magnetite/maghemite (SAED). Mössbauer results at 80 K showed line shapes dominated by magnetic relaxation effects with sextets and combinations of sextets and doublets due to the asymmetric line shapes and very large broadening of sextets. The hyperfine parameters revealed the presence of Fe^{3+}, and small amounts of Fe^{2+} for the dried samples, which indicates a sample oxidation during the drying process. The doublet features dominated the samples obtained at pH 10. Also, the Mössbauer spectra showed effects of interparticle interactions leading to the presence of sextets, especially for pH 12 samples, due to high density of particles embedded in the surfactant which is increased by the drying process. This fact can be understood considering that the particle size, from XRD and TEM, is in the average range of 5-10 nm; in this way, it is expected a doublet component at 80 K which is missing.

The interactions of the surfactant with the nanoparticle surface, mainly with the Fe^{3+}, are strong, showing at least two surfactant layers: one layer directly over the nanoparticle surface and another layer resting over the inner layer. The frequency shifts, intensity, and line shape changes in FTIR confirmed the attachment of the surfactant to the magnetic nanoparticle surface. The main mechanism of binding for the protein was the chelating mechanism, due to the fact that both particles and surfactant present a negative charge which leads to repulsion forces between them.

The magnetic behavior was evaluated in gel form by moment versus temperature, and magnetic field measurements. The nanoparticles showed superparamagnetic behavior at room temperature and are blocked at 5 K. The saturation magnetization presented lower values than reported bulk values and nanosystems prepared by a different route, due to the presence of a large layer of maghemite. A magnetic diameter was estimated from the initial susceptibility which shows very close values for all samples indicating that at these one-step synthesis conditions, especially large concentrations 1-3 % (m/m), the particle growth proceeds in a similar way. The FC/ZFC magnetization curves confirmed the superparamagnetic nature of the iron oxide particles and

showed that the distribution of moments was broad for pH 12 samples while it was narrow for pH 10 samples. The magnetic information deduced from Mössbauer spectroscopy confirms the magnetic information extracted from magnetic measurements.

The very close particle size, from each method separately, obtained from XRD, TEM, and magnetic measurement, gave indication that the particle growth was dominated by the surface properties of the nanoparticles and that the very different synthesis conditions did not affect the growth process.

ACKNOWLEDGMENTS

The authors are grateful to Colciencias, Colombian research Council, and CODI, Sustainability Program for Solid State Group 2011-2012, Universidad de Antioquia, for financial support.

REFERENCES

Alexandrescu, R.; Morjan, I.; Dumitrache, F.; Scarisoreanu, M.; Soare, I.; Fleaca, C.; Birjega, R.; Popovici, E.; Gavrila, L.; Prodan, G.; Ciupina, V.; Filoti, G.; Kuncser, V. and Vekas, L. (2008). Photochemistry Aspects of the Laser Pyrolysis Addressing the Preparation of Oxide Semiconductor Photocatalysts. *International Journal of Photoenergy*, 2008, pp. 1-11.

Amemiya, Y.; Arakaki, A.; Staniland, S.S.; Tanaka, T.; Matsunaga, T. (2007). Controlled Formation of Magnetite Crystal by Partial Oxidation of Ferrous Hydroxide in the Presence of Recombinant Magnetotactic Bacterial Protein Mms_6. *Biomaterials*, 35(28) December, pp. 5381-5389.

Barbeta, V. B.; Jardim, R. F.; Kiyohara, P. K.; Effenberger, F. B.; Rossi, L. M. (2010). Magnetic Properties of Fe_3O_4 Nanoparticles Coated with Oleic and Dodecanoic Acids. *Journal of Applied Physics*, 107(7), pp. 073913- 073913-7

Barth, A. (2007). Infrared Spectroscopy of Proteins. *Biochimica et Biophysica Acta*, 1767(9) September, pp. 1073–1101.

Barth, A.; Zscherp, C. (2000). Substrate Binding and Enzyme Function Investigated by Infrared Spectroscopy. *Febs Letters*, 477(3), pp. 151–156.

Dallas, P.; Georgakilas, V.; Niarchos, D.; Komninou, P.; Kehagias, T.; Petridis, D. (2006). Synthesis, Characterization and Thermal Properties of Polymer/Magnetite Nanocomposites. *Nanotechnology*, vol. 17(8), pp. 2046–2053.

Dong Cheng, powderx. Institute of Physics, Chinese Academy of Sciences. P. O. Box 603, Beijing 100080

Doriguetto, A.C.; Fernandes, N. G.; Persiano, A. I. C.; Nunes Filho, E.; Greneche, J. M.; Fabris, J. D (2003). Characterization of a Natural Magnetite. *Physics and Chemistry of Minerals*, 30(5), pp. 249-255.

Goss C. J. (1988). Saturation Magnetisation, Coercivity and Lattice Parameter Changes in the System Fe_3O_4-$\gamma Fe2O_3$, and their Relationship to Structure. *Physics and Chemistry of Minerals*, 16(2) November, pp. 164-171.

Goya, G.F. (2004). Handling the Particle Size and Distribution of Fe_3O_4 Nanoparticles Through Ball Milling. *Solid State Communications*, 130, pp. 783–787

Gupta Ajay Kumar, Gupta Mona (2005). Synthesis and Surface Engineering of Iron Oxide Nanoparticles for Biomedical Applications. *Biomaterials*, 26, pp. 3995–4021.

Haiping Qi; Jing Ye; Nan Tao; Minghua Wen; Qianwang Chen (2009). Synthesis of Octahedral Magnetite Microcrystals with High crystallinity and Low Coercive Field, *Journal of Crystal Growth*, 311(2), pp. 394–398

Harris, L. A.; Goff, J. D.; Carmichael, A. Y.; Riffle, J. S.; Harburn, J. J.; Pierre, T. G. St.; Saunders, M. (2003). Magnetite Nanoparticle Dispersions Stabilized with Triblock Copolymers, *Chemical Mater*, 15(6), pp.1367-1377.

Herzera, G.; Vázquez, M.; Knobelc, M.; Zhukovd, A.; Reiningere, T.; Daviesf, H.A.; Grössingerg, R.; Sánchez-Ll., J.L. (2005). Round Table Discussion: Present and Future Applications of Nanocrystalline Magnetic Materials. *Journal of Magnetism and Magnetic Materials*, 294(2), pp. 252–266

Huang Jing; Wang Liya; Lin Run; Wang Andrew Y.; Yang Lily; Kuang Min; Qian Weiping; Mao Hui (2013). Casein-Coated Iron Oxide Nanoparticles for High MRI Contrast Enhancement and Efficient Cell Targeting. *ACS Applied Materials and Interfaces*, 5(11), pp.4632-4639.

Koong, Jilie; Yu, Shaoning (2007). Fourier Transform Infrared Spectroscopic Analysis of Protein Secondary Structures. *Acta Biochimica et Biophysica Sinica*, 39(8), pp. 549–559.

Lima Jr., E.; De Biasi, E.; Vásquez-Mansilla, M.; Saleta, M. E.; Effenberg, F.; Rossi, L. M.; Cohen, R.; Rechenberg H. R.; Zysler, R. D. (2010). Surface Effects in the Magnetic Properties of Crystalline 3 nm Ferrite

Nanoparticles Chemically Synthesized. *Journal Applied Physics*, 108(10), pp. 103919.

Lin Chia-Lung; Lee Chia-Fen; Chiu Wen-Yen (2005). Preparation and Properties of Poly(acrylic acid) Oligomer Stabilized Superparamagnetic Ferrofluid. *Journal of Colloid and Interface Science*, 291(2), pp. 411–420.

Morales, A.L.; Velásquez, A. A.; Urquijo, J. P.; Baggio, E. (2011). Synthesis and Characterization of Cu_2+ Substituted Magnetite. *Hyperfine Interactive*, 203(1-3), pp. 75–84.

Nadeem, K.; Krenn, H.; Traussnig, T.; Wurschum, R.; Szabo, D.V.; Letofsky-Papst, I. (2011). Effect of Dipolar and Exchange Interactions on Magnetic Blocking of Maghemite Nanoparticles. *Journal of Magnetism and Magnetic Materials*, 323(15), pp.1998–2004

Novakova, A.A.; Smirnov, E.V.; Gendler, T.S. (2006). Magnetic Anisotropy in Fe_3O_4—PVA nanocomposites as a result of Fe_3O_4-Nanoparticles Chains Formation. *Journal of Magnetism and Magnetic Materials*, 300(1), pp. e354–e358.

Parker, D.; Ladieu, F.; Vincent, E.; Mériguet, G.; Dubois, E.; Dupuis, V.; Perzynski, R. (2005). Experimental Investigation of Superspin Glass Dynamics. *Journal of Applied Physics*, 97(10), pp. 10A502-10A502-3.

Prozorov, T.; Mallapragada, S. K.; Narasimhan, B.; Wang Lijun; Palo, P.; Nilsen-Hamilton, M.; Williams, T. J.; Bazylinski, D. A.; Prozorov, R.; Canfield, P. C. (2007). Protein-Mediated Synthesis of Uniform Superparamagnetic Magnetite Nanocrystals. *Advanced Functional Material*, 17, pp. 951–957

Quantum Design, application note. http://www.qdusa.com/sitedocs/appNotes/ppms/1070-207.pdf

Rebodos, R. L.; Vikesland, P. J. (2010). Effects of Oxidation on the Magnetization of Nanoparticulate Magnetite. *Langmuir*, 22(26), pp. 16745–16753.

Roca, A.G.; Costo, R.; Rebolledo, A.F.; Veintemillas-Verdaguer, S.; Tartaj, P.; Gonzalez-Carreño, T.; Morales M.P.; Serna, C.J. (2009). Progress in the preparation of magnetic nanoparticles for applications in biomedicine. *Journal Physics D: Applied Physics*, 42(22), pp. 224002.

Slavov, L.; Abrashev, M.V.; Merodiiska, T.; Gelev, Ch.; Vandenberghe, R.E.; Markova-Deneva, I.; Nedkov, I. (2010). Raman Spectroscopy Investigation of Magnetite Nanoparticles in Ferrofluids. *Journal of Magnetism and Magnetic Materials*, 322, pp. 1904–1911.

Soler Maria A. G.; Qu Fanyao. Raman Spectroscopy of Iron Oxide Nanoparticles. Challa S. S., R. Kumar (ed.), Raman Spectroscopy for Nanomaterials Characterization, Springer-Verlag Berlin Heidelberg, 2012.

Sugiarto M., Ye A., Singh H. (2009). Characterisation of Binding of Iron to Sodium Caseinate and Whey Protein Isolate. *Food Chemistry*,114(3) June, pp. 1007–1013

Vandenberghe, R.; De Grave, E.; De Bakker, P. M. A. (1994). On the Methodology of the Analysis of Mössbauer Spectra. *Hyperfine Interactions*, 83, pp. 29-49

Zhai, Yongai; Liu, Fengqi; Zhang, Qing,;Gao Ge (2009). Synthesis of Magnetite Nanoparticle Aqueous Dispersions in an Ionic Liquid Containing Acrylic Acid Anion. *Colloids and Surfaces A: Physicochem Enginnering Aspects*, 332(1-3), pp. 98–102.

Zhang, J.L.; Srivastava, R.S.; Misra, R.D.K. (2007). Core-Shell Magnetite Nanoparticles Surface Encapsulated with Smart Stimuli-Responsive Polymer: Synthesis, Characterization, and LCST of Viable Drug-Targeting Delivery System. *Langmuir*, 23(11), pp. 6342-6351

PARA CITAR ESTE ARTÍCULO / TO REFERENCE THIS ARTICLE / PARA CITAR ESTE ARTIGO /

Urquijo-Morales, J.P.; Casanova-Yepes, H.; Morales-Aramburo, A.L.; Zysler, R.D. (2014). One Step Synthesis of Magnetic Particles Covered with Casein Surfactant. *Revista EIA*, 11 (Edición especial N.1) marzo, pp. 47-59. [Online]. Disponible en: http://dx.doi.org/10.14508/reia.2014.11.e1.47-59